J Mater Sci: Mater Electron (2013) 24:4566–4573
DOI 10.1007/s10854-013-1443-4

Breaking point of the harmony between Gd diffused Bi-2223 slabs with diffusion annealing temperature

H. Aydın · A. Babanli · S. P. Altintas · E. Asikuzun · N. Soylu · O. Ozturk · M. Dogruer · C. Terzioglu · G. Yildirim

Received: 12 July 2013 / Accepted: 8 August 2013 / Published online: 21 August 2013

Abstract This comprehensive study reports the role of annealing temperature on the microstructural, superconducting and mechanical characteristics of the Gd diffused Bi-2223 superconducting ceramics produced by the conventional solid-state reaction route at 840 °C for the annealing duration of 48 h. For the material characterization, the standard experimental methods such as dc resistivity (ρ-T), transport critical current density, X-ray powder diffraction, scanning electron microscopy and Vickers microhardness measurements are performed systematically. All the results obtained show that all the measured characteristic properties, being in charge of the applications in the industry, engineering and technology, improve until a certain diffusion annealing temperature of 800 °C beyond which they tend to degrade considerably. The increase in the properties is mostly related to the transition from the inherent overdoped state of the pure Bi-2223 material to optimum doped state with the diffusion annealing temperature, confirming the penetration of the sufficient Gd nanoparticles into the crystal structure. On the other hand, the suppression in the superconducting properties stems from the appearance of the porosity, defects, disorder and localization problem in the polycrystalline Bi-2223 superconducting matrix. This is attributed to the decrement of the average crystallite size and mobile hole concentration in the Cu–O_2 layers and especially the retrogression of the crystallinity in the system. As for the mechanical characteristics, Vickers microhardness measurements exerted in the applied indentation test load range of 0.245–2.940 N indicate that the Gd diffused bulk superconducting samples exhibit the typical indentation size effect behavior. With the enhancement in the annealing temperature up to 800 °C, the significant increase in the elastic modulus, yield strength and fracture toughness is one of the most striking points in the paper. The long and short of it is that the excess diffusion annealing temperature damages the fundamental characteristics of the Bi-2223 system.

1 Introduction

Over the past decades, Bi-based superconducting samples have attracted considerable interest in science, material synthesis and optical and electronic productions due to the remarkable smaller power losses, high current and magnetic field carrying capacity [1–4]. Moreover, the materials composed of the layered (consecutively stacked) structures confine the charge carriers in the Cu–O_2 planes and so play important role in the electronical and technological applications [5]. In the Bi-based family, three (n=1, 2 and 3) different superconducting phases appear with respect to the number of the Cu–O_2 layers in the unit cell. Among the phases, the Bi-2223 one (n=3) is superior to the others as a consequence of the highest critical temperature and critical

H. Aydın · A. Babanli
Department of Physics, Suleyman Demirel University, 32100 Isparta, Turkey

S. P. Altintas · N. Soylu · M. Dogruer · C. Terzioglu (✉)
Department of Physics, Abant Izzet Baysal University, 14280 Bolu, Turkey
e-mail: terzioglu_c@ibu.edu.tr

E. Asikuzun · O. Ozturk
Department of Physics, Kastamonu University, 37100 Kastamonu, Turkey

G. Yildirim
Department of Mechanical Engineering, Abant Izzet Baysal University, 14280 Bolu, Turkey

current density [6–8]. On the other hand, the researchers sometimes encounter the trouble problems due to the high complexity of the reaction and the appearance of numerous phases as Bi-2212 (n=2), Bi-2201 (n=1) and Ca_2PbO_4 during the phase formation [9]. Thus, the Bi-2223 superconducting sample prepared has weak link problems and inadequate for the preparation of long wires and tapes with high critical current densities [10]. In fact, the inherit brittleness nature much more appears and the material is greatly limited for the potential mechanical applications [11]. As a result, much effort has been focused on preparation conditions to overcome these kinds of problems, because the Bi-2223 is an indispensable phase for the potential engineering application. In the present work, we struggle to produce the high quality Bi-2223 phase with the aid of the Gd individuals penetrated into the crystal structure. The full characterization of the samples is performed by the dc electrical resistivity, transport critical current density, scanning electron microscopy, X-ray diffraction and microhardness experiments. All the findings show that the diffusion annealing temperature up to the certain value of 800 °C positively affects the properties given above. However, after the critical value they start to degrade due to the incorporation of the excess Gd inclusions into the Bi-2223 superconducting matrix.

2 Experimental procedure

This study is composed of two experimental parts. In the first part, we produce the $Bi_{1.8}Pb_{0.35}Sr_{1.9}Ca_{2.1}Cu_3O_y$ (Bi-2223) superconducting ceramics via the conventional solid-state reaction method using the high-purity (99.9%) starting chemicals of Bi_2O_3, PbO, $SrCO_3$, $CaCO_3$ and CuO (Alfa Aesar Co., Ltd.). The chemicals weighed in stoichiometric proportion are grinded for the duration of 12 h to obtain homogeneous mixture of ingredients. The resultant mixture is pelletized into the rectangular bar of 1.5 × 0.5x0.2 cm^3 in the air atmosphere at 250 MPa at room temperature. The solidified products are sintered at the constant temperature of 840 °C for 48 h. Both the heating and cooling rates of the temperature are chosen to be 5 °C/min. The second part is related to the diffusion of the Gd impurities on the specimens. The GdF_3 chemical (Alfa Aesar Co., Ltd. 99.99% purity) is used as a target material when an AUTO 306 vacuum coater (EDWARDS) carries out the Gd diffusion under the pressure of $2.67e^{-4}$ Pa. After taking the samples out, the color of silvery-white residues on the (blackish) products confirms that the Gd diffusion is perfectly carried out. The average thickness of the impurities is measured to be about 30 μm. The final products are exposed to the annealing process in the air atmosphere at different temperature (650, 700, 750, 800 and 840 °C). The superconducting ceramics produced will hereafter be given as Gd-650, Gd-700, Gd-750, Gd-800 and Gd-840, respectively. For the characterization of the samples, dc resistivity, transport critical current density, X-ray diffraction, scanning electron microscopy and Vickers microhardness measurements are performed systematically.

Dc resistivity measurements are performed by the standard four-point technique using 5 mA dc current throughout the specimen surface in the He gas contact (closed-cycle) cryostat in the temperature range from 80 to 125 K. The measurement system includes a Keithley 220 programmable current source and a Keithley 2182A nano-voltmeter system. The experimental findings are recorded by Labview software. Besides, we measure the transport critical current measurements in the self-field using four-probe method in the home-made system at the liquid nitrogenous (77 K) in zero magnetic field. The J_c values of the samples are determined for a standard criterion of 1 μV/cm.

X-ray powder diffraction measurements are exerted by a Rigaku Multiflex+XRD diffractometer, equipped with a curved graphite monochromate using CuK_α radiation (1.54 Å), in the range of 2θ = 4–70° at a scanning rate of 3°/min and step increment of 0.02° at room temperature in air atmosphere. The operation is carried out at 38 kV and 28 mA. The XRD curves obtained allow us to calculate the lattice constant parameters (with the accuracy of ±0.0001 Å) and volume fraction values. The average crystallite size is also determined from the Scherrer–Warren approach.

As for the SEM investigations, the surface morphology, grain size distribution, connectivity between the superconducting grains and grain boundary weak-links in the Gd diffused Bi-2223 bulk superconductors are determined using a Jeol scanning electron microscope JEOL 6390-LV, operated at 20 kV, with a resolution power of 3 nm.

Moreover, Vickers hardness tests are conducted on the specimen surface at room temperature in the air atmosphere with the aid of a digital microhardness tester (SHIMADZU, HVM-2). The indentation test load is applied for 10 s in the load range from 0.245 to 2.940 N. The measurements are performed at various regions of the specimen surfaces due to the overlap problem of the indentations. The independent Vickers microhardness, elastic modulus, yield strength and fracture toughness values are also inferred from the experimental plots.

3 Result and discussion

3.1 Electrical experimental findings

Temperature-dependent dc electrical resistivities of the pure and Gd diffused polycrystalline superconductors are

graphically displayed in the temperature range of 80–125 K in Fig. 1. As seen from the figure that with the increase of the diffusion annealing temperature the conspicuous changes in the resistivity value and transition are observed clearly although each sample obtains a sharp or broad transition into the superconducting state below the onset critical transition temperature with the positive resistivity-temperature coefficient (dρ/dt) due to the electron-phonon interaction [12, 13] or logarithmic divergence in density of states at the Fermi level [14–16]. Even, the positive temperature coefficient of the resistivity is related to the metallic behavior (linear temperature- dependent resistivity) of the material. Figure 1 also shows that the normal state resistivity values (after the onset temperature) rapidly decrease as the diffusion annealing temperature systematically increases from 650 to 800 °C beyond which the resistivity tends to increase slowly again, however. The decrement in the conductivity for higher annealing temperature value is attributed to the retrogression of the optimization of the mobile hole density and possible changes in the lattice vibration [17, 18], leading to the degradation of the metallic connection between the Bi-2223 superconducting slabs. In other words, the change of the resistivity with the annealing temperature indicates the transition from inherently overdoped state of the pure sample to optimally doped (or underdoped) state of the Gd diffused ones [19–22]. According to the figure, the resistivity of the pure sample (overdoped state) is threefold higher than that of the Gd-800 sample (optimally doped). Moreover, we deduce the onset critical transition (T_c^{onset}) and offset critical transition (T_c^{offset}) temperatures from the same figure. Similar to the conductivity, both the temperature values increase with the diffusion annealing temperature up to 800 °C, after the critical point, the values start to decrease notably. Regardless, the conductivity results of the (pure) sample prepared at 840 °C for 48 h are superior to the pure sample. Namely, the smallest T_c^{onset} of 112.6 and T_c^{offset} of 95.9 K are observed for the pure sample while the higher T_c^{onset} and T_c^{offset} values are obtained to be about 113.9 and 105.2 K for the Gd-800 sample, respectively (Table 1). The Gd-840 sample also exhibits the T_c^{onset} of 113.4 and T_c^{offset} of 101.3 K. These results confirm that the diffusion annealing temperature of 800 °C is the best condition for the feasibility of obtaining Gd diffused Bi-2223 bulk superconducting material with its tailored structure. Besides, for the samples prepared in this work, there is a rapid enhancement of the T_c^{offset} values over slight increment in the T_c^{onset} values. This phenomenon causes to the decrease in the degree of the broadening ($\Delta T_c = T_c^{onset} - T_c^{offset}$), meaning the existence of homogeneities in the oxidation states of the superconducting grains [23]. Thus, it would be more precise to say that the negative effects on the conductivity properties such as the porosity, defects, stacking faults, grain boundary weak-links, grain mis orientations and especially the divergence from the optimization of the hole concentration tend to decrease monotonously with the increase of the diffusion annealing temperature up to 800 °C [24–26].

3.2 Carrier concentration calculation

Mobile hole carrier (hole filling) concentration per Cu ion (P) in the conduction band is a special parameter to characterize the alteration of the superconducting properties and can be determined from the following equation [27].

$$P = 0.16 - \left[\left(1 - \frac{T_c^{offset}}{T_c^{\max}}\right)/82.6\right]^{1/2} \quad (1)$$

where $T_c^{\max}$ is used as 110 K for the high-Tc phase [28] and the T_c^{offset} values are extracted form Table 1. The mobile hole concentration values computed are numerically given in Table 1. It is obvious from the table that the maximum value of 0.144 is attributed to the Gd-800 sample whereas the minimum (0.118) is noted for the pure sample. This enhancement of the concentration level in the conduction band is in accordance with the exchange scattering of the mobile holes owing to the magnetic moments of the Gd impurities in the Bi-2223 superconducting core [29, 30].

3.3 XRD evidences

In this part of the paper, we focus on the change of the crystal plane alignment (texturing), phase purity, crystal structure, crystallite (grain) size and lattice constant parameters as a consequence of the introduction of the Gd additives into the Bi-2223 crystal structure. In Fig. 2, one can examine the room temperature powder X-ray

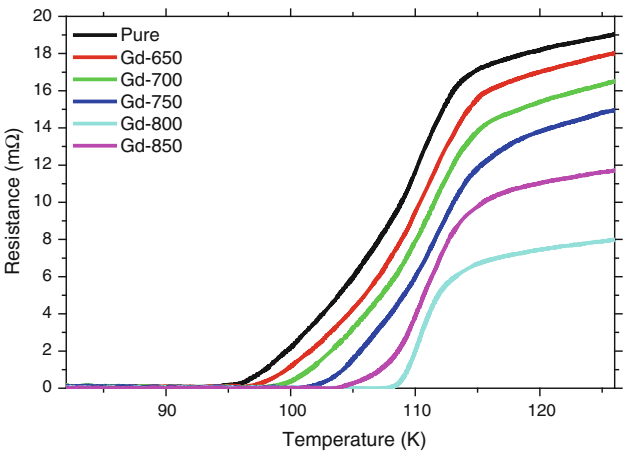

Fig. 1 Temperature-dependent resistivity curves for the samples studied

Table 1 *XRD* and transport measurement results belonging to the samples

Samples	a (Å)	c (Å)	Volume fraction (%) 2223–2212	T_c^{offset} (K)	T_c^{onset} (K)	ΔT_c (K)	Mobile hole concentration P	Grain size (nm)	J_c A.cm^{-2}
Pure sample	5.39	31.11	42 58	95.9	112.6	16.7	0.118	25.55	794
Gd-650C	5.38	31.23	47 53	96.2	112.8	16.6	0.120	27.97	1,335
Gd-700C	5.37	32.06	49 51	97.4	113.1	15.7	0.122	36.03	1,979
Gd-750C	5.36	32.65	57 43	98.5	113.3	14.8	0.123	37.67	2,503
Gd-800C	5.32	37.92	83 17	105.2	113.9	8.7	0.144	58.73	3,822
Gd-840C	5.33	34.71	68 32	101.3	113.4	11.1	0.130	48.15	3,101

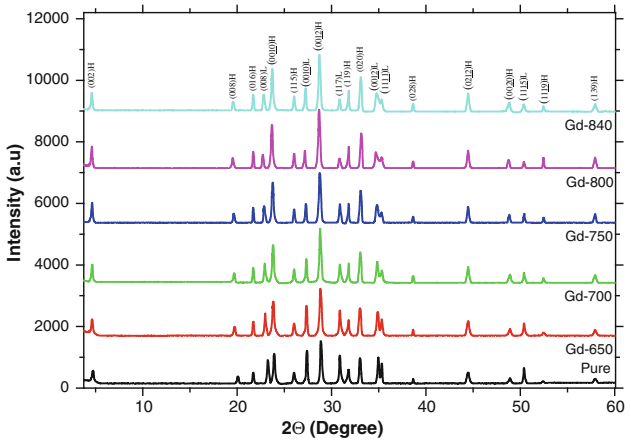

Fig. 2 *XRD* patterns of the Bi-2223 superconducting materials

diffraction patterns ranging from 3 to 60° for all the superconducting samples. Before starting the discussions, it is necessary to underline that no secondary phase belonging to Gd impurities and any other cationic groups is not encountered for all the samples studied. Thus, it is not wrong to claim that the diffused particles are thoroughly entered into the Bi-2223 system and solved completely [31–35]. As for the detailed examinations, the characteristic peaks belonging to the low-T_c (Bi-2212) and high-T_c (Bi-2223) phases are signed as H(*hkl*) and L(*hkl*) Miller indices. It is apparent from the figure that the formation of the low-T_c and high-T_c phase velocity strongly depends on the diffusion annealing temperature, resulting in the incorporation of more and more Gd inclusions into the grains or over grain boundaries in the superconducting matrix. These results are also confirmed by the variation of the diffraction line intensities. Namely, the well defined diffraction peaks (*002*, *008*, *0010* and *0012*) corresponding to the Bi-2223 superconducting phase improve systematically with the enhancement of the diffusion annealing temperature up to 800 °C beyond which the peaks tend to degrade considerably as a result of the retrogression in the crystallinity and crystal plane alignments. This is related to the excessive accumulation of the Gd individuals in the Bi-2223 superconducting core. Regardless, the Bi-2223 peak intensities of the sample prepared at diffusion annealing temperature of 840 °C are superior to those of the pure sample. Thus, we do not need to give the other experimental results (except for the transport measurement evidences) belonging to the undiffused sample. The relative phase change is also computed from the following relations.

$$f_{(2223)} = \frac{\sum I_{H(hkl)}}{\sum I_{H(hkl)} + \sum I_{L(hkl)}} \text{ (for high} - T_c \text{ phase)} \quad (2)$$

$$f_{(2212)} = \frac{\sum I_{L(hkl)}}{\sum I_{H(hkl)} + \sum I_{L(hkl)}} \text{ (for low} - T_c \text{ phase)} \quad (3)$$

where I denotes the peak intensity value. The relative percentages belonging to the high and low phases are numerically listed in Table 1. According to the table, the high phase regularly increases from % 42 to % 83 with the diffusion annealing temperature up to the certain point of 800 °C after which the phase level decreases to % 68. This is attributed to the fact that the excess diffusion annealing temperature damages the crystallinity and texturing of the Bi-based superconducting ceramics because of the penetration of more and more Gd inclusions into the crystal structure. Similar results can be observed in electrical measurement part.

At the same time, the variation of the lattice constant parameters is easily observed from the shift of the characteristic peaks in the XRD patterns. We calculate the lattice parameters by using the least square method by means of the d values and (*h k l*) planes in the tetragonal unit cell structure. The calculated parameters for each sample are tabulated in Table 1. As seen from the table, the length of the c-axis initially expands from 31.11 to 37.92 Å with the increase in the diffusion annealing temperature up to 800 °C; however, the parameter interestingly contracts to 34.71 Å for the sample prepared at the annealing temperature of 840 °C for 48 h. Conversely, the largest a parameter of 5.39 Å is calculated for the pure sample whereas the smallest one (5.32 Å) is attributed to the Gd-800 sample. According to the results, the best crystallinity

is observed for the diffusion annealing temperature of 800 °C for 48 h. In other words, for the annealing temperature there is critical point such as 800 °C excess of which the formation velocity of the Bi-2223 phase starts to degrade significantly.

Additionally, the determination of the crystallite size from the XRD peak broadenings (presenting the nanocrystalline formation) is another advantage for the superconducting materials. The size of the superconducting grains is useful tool to provide the formal information about the degradation or improvement in the formation velocity of the Bi-2223 phase and can be calculated by the following relation [36]

$$t = {}^{0.941\lambda}/_{B\cos\theta_B} \quad (4)$$

where t denotes the crystal thickness, λ is the wavelength and B ($B^2 = B_m^2 - B_s^2$) indicates the full width at half maximum (FWHM), B_s is attributed to the half width of the standard material in radian, and θ_B is the Bragg angle. One can see the calculated grain size values in Table 1 in detail. It is apparent from the table that the crystallite size regularly enhances from 25.55 to 58.73 nm with the increase of the annealing temperature up to 800 °C. This is associated with the fact that the annealing temperature initially affects positively the superconducting properties of the Bi-2223 bulk superconductors as a result of the optimum Gd dopant concentration. However, the excess annealing temperature leading to the penetration of more and more Gd inclusions into the Bi-2223 crystal structure damages radically the superconducting properties.

3.4 SEM examinations

The microstructural changes in the surface morphology, crystallinity, texturing, grain size distribution and connectivity between the superconducting grains with the Gd decorations on the specimens are studied by scanning electron microscopy (SEM) experiments in the secondary electron image mode at 3000 × magnification. Moreover, possible precipitation at the grain boundaries (increase in the weak-links or not) is examined in detail. One can see the typical SEM images pictured from the specimen surfaces in Fig. 3. It is natural to say that the microstructural characteristics are curicially dependent upon the diffusion annealing temperature. In particular, the particle (crystalline) size increases systematically with the diffusion annealing temperature up to the critical point of 800 °C beyond which the dense surface with a fine connectivity between the Bi-2223 superconducting grains suppresses considerably. It means that there is a critical annealing temperature value such as 800 °C where the Bi-2223 material has the smoothest and densest (least weak links between the superconducting grains) surface morphology. In other words, the diffusion annealing temperature of 800 °C is favorable for the Bi-2223 superconducting phase owing to the increase of the harmony between Bi-2223 layers. After the critical point, the microstructural characteristics begin to degrade monotonously and maybe reach the worst morphology at the higher diffusion annealing temperature as a consequence of the incorporation of the excess Gd impurities into the Bi-2223 crystal structure. Similar results for the different superconducting systems are encountered in the literature [10, 37–39].

3.5 Transport critical current density investigations

Pinning mechanism of the polycrystalline superconducting materials studied in this work is examined by means of the transport critical current density (J_c) measurements. The discussion on the curves also enables us to determine the quality of the connectivity between superconducting grains in the Bi-2223 crystal structure [40]. The J_c values obtained are provided in Table 1. As seen from the figure, similar to the resistivity evidences, the values increase with the increase from 794 to 3,822 A.cm^{-2} with the diffusion annealing temperature up to 800 °C after which the J_c value again decreases to 3,101 A.cm^{-2}. The increase in the value stems from the introduction of the flux pinning centers into the crystal structure via the Gd inclusions [41, 42].

3.6 Vickers microhardness measurements

This part of the paper deals with the mechanical properties of the Gd diffused Bi-2223 superconductors, exposed to the different annealing temperature, by means of the Vickers microhardness measurements in the test load range of 0.245–2.940 N. The real (true) microhardness (H_v), elastic (Young's) modulus (E), yield strength (Y) and fracture toughness (K_{IC}) parameters are deduced from the Vickers measurement curves by using the following equations.

$$H_V = 1.8544\left(\frac{F}{d^2}\right) \quad (5)$$

$$E = 81.9635H_V \quad (6)$$

$$Y \approx \frac{H_V}{3} \quad (7)$$

$$K_{IC} = \sqrt{2E\gamma} \quad (8)$$

in the relations, F displays the applied indentation test load, γ denotes surface energy and d (in the unit of μm) ascribes to the mean diagonal length of the indentation impression. One can find the H_v values in Fig. 4 easily. Based on the figure, each sample exhibits the non-linear microhardness

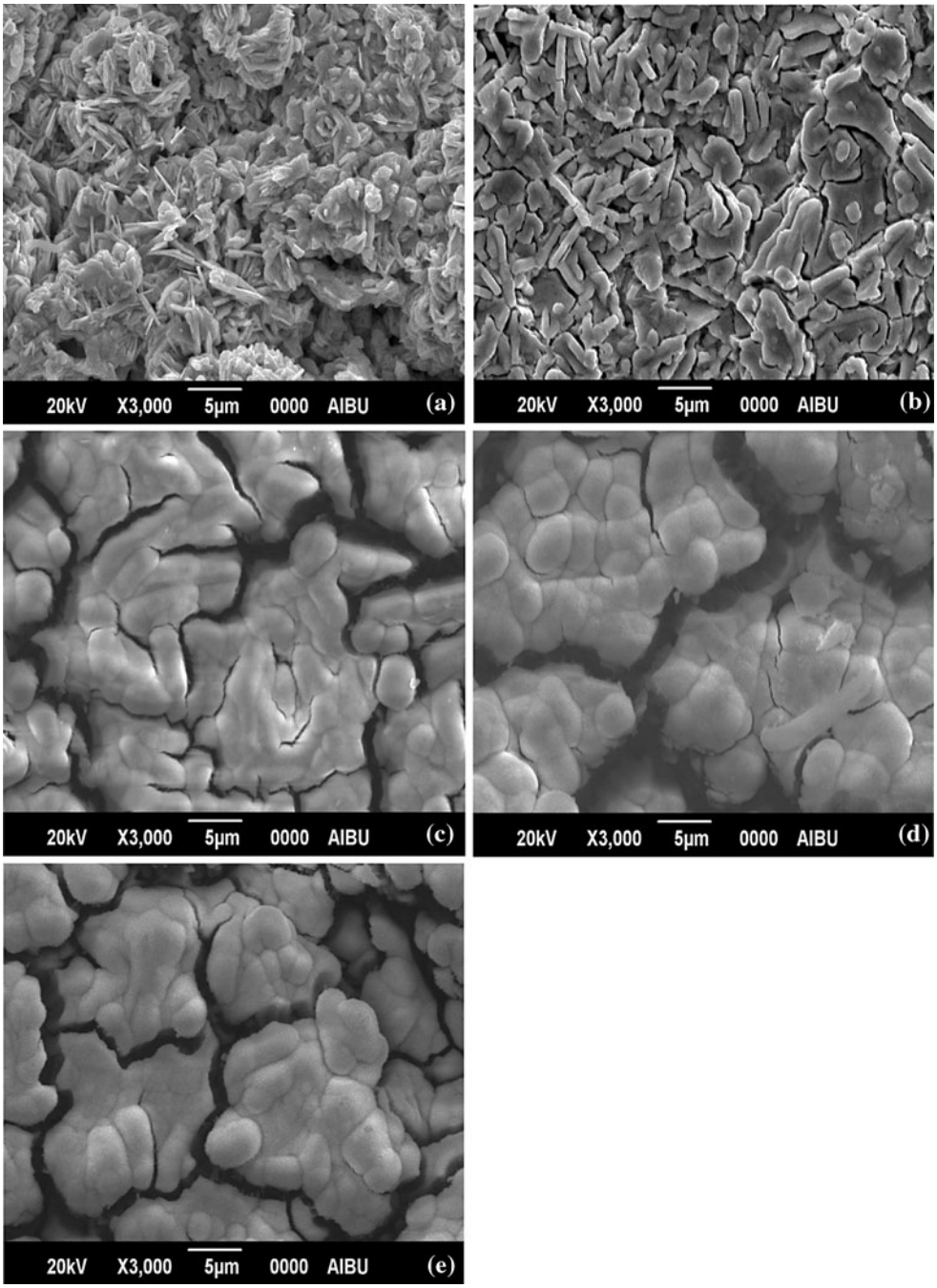

Fig. 3 *SEM* images for **a** Gd-650 **b** Gd-700 **c** Gd-750 **d** Gd-800 and **e** Gd-840 samples

behavior and the H_v values decrease with the increment of the applied load. This behavior is called as the typical indentation size effect (*ISE*) and the elastic recovery plays dominant character on the samples prepared. In other words, both the elastic (reversible) and plastic (irreversible) deformations are observed simultaneously in the polycrystalline ceramics. Moreover, the Hv values at all the test loads for the Gd-800 sample are found to be much greater as compared to those of the others. This is attributed to the fact that the least specimen cracking/porosity, grain boundary weak-links and irregular grain orientation distribution [40] are observed for the sample, favored by the XRD and SEM results. The similar trend is also seen in the elastic (Young's) modulus (E), yield strength (Y) and fracture toughness (K_{IC}) parameters (Table 2). All in all, the crystallinity and the strength in the interaction between the grains improve with the diffusion annealing temperature up to 800 °C, above the value of which damages the

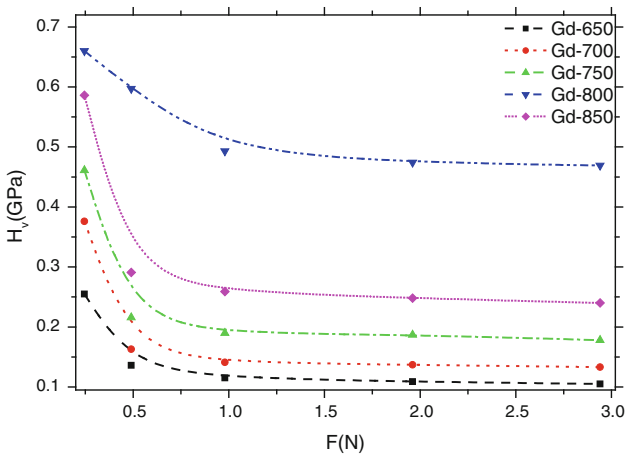

Fig. 4 The variations of microhardness with respect to the applied test load for the samples, exposed to the Gd diffusion

Table 2 The calculated true H_v, E, Y and K_{IC} parameters for the samples

Samples	F (N)	d_{ort} (μm)	H_v (GPa)	E (GPa)	Y (GPa)	K_{ic} (Pa/m$^{1/2}$)
Gd-650C	0.245	42.28	0.255	20.90	0.085	365.73
	0.490	81.62	0.136	11.14	0.045	267.01
	0.980	125.49	0.115	9.425	0.038	245.60
	1.960	182.13	0.109	8.934	0.036	239.12
	2.940	227.91	0.105	8.606	0.035	234.69
Gd-700C	0.245	34.82	0.376	30.81	0.125	496.47
	0.490	75.04	0.163	13.36	0.054	326.93
	0.980	113.55	0.141	11.55	0.047	303.97
	1.960	163.85	0.137	11.22	0.045	299.60
	2.940	203.49	0.133	10.90	0.044	295.30
Gd-750C	0.245	31.43	0.461	37.78	0.153	570.01
	0.490	64.99	0.216	17.70	0.072	390.15
	0.980	97.71	0.190	15.57	0.063	365.93
	1.960	139.19	0.187	15.32	0.062	362.98
	2.940	175.91	0.178	14.59	0.059	354.22
Gd-800C	0.245	26.22	0.660	54.09	0.220	624.06
	0.490	39.07	0.597	48.93	0.199	593.55
	0.980	60.81	0.493	40.40	0.164	539.33
	1.960	87.54	0.474	38.85	0.158	528.89
	2.940	108.01	0.469	38.44	0.156	526.09
Gd-840C	0.245	27.83	0.586	48.03	0.195	671.92
	0.490	55.84	0.291	23.85	0.097	473.49
	0.980	83.96	0.259	21.22	0.086	446.62
	1.960	121.39	0.248	20.32	0.082	437.04
	2.940	150.59	0.240	19.67	0.080	430.00

mechanical properties of the Gd diffused Bi-2223 superconducting materials due to the penetration of the excess (Gd) impurities into the Bi-2223 system.

4 Conclusion

In the current work, the standard characterization methods such as ρ-T, J_c, XRD, SEM and H_v measurements enable us to manifest the positive effect of the diffusion annealing temperature up to the critical value of 800 °C on the electrical, mechanical, microstructural and superconducting characteristics of the polycrystalline Gd diffused Bi-2223 superconducting materials. The importance findings deduced from the work are the following.

- The dc resistivity measurements show that all the samples exhibit the metallic behavior as a result of the presence of the electron-phonon interaction in the crystal lattice or logarithmic divergence in density of states at the Fermi level. With the enhancement of the diffusion annealing temperature, the normal state resistivity value begins to decrease monotonously and in fact reaches the local minimum point for the annealing temperature of 800 °C beyond which the value increases due to both the degradation of the optimization of the mobile hole density (transition of the Bi-2223 system to underdoped state) and the increase of the porosity, stacking faults, disorder and voids in the system.
- The similar variation is observed for the T_c^{onset} and T_c^{offset} values. Both values reach the maximum points (113.9 K and 105.2 K, respectively) for the sample produced at the diffusion annealing temperature of 800 °C, leading to the decrement in the degree of the transition broadening. This is attributed to the reduction of the grain boundary weak-links, grain misorientations and the divergence from the optimization of the hole concentration.
- Based on the J_c results, the sufficient Gd inclusions (highly dispersed particles) inserted in the Bi-2223 superconducting core form the flux pinning centers through the crystal structure and so the J_c value increases considerably with the annealing temperature.
- The XRD findings confirm that the diffused particles are thoroughly introduced into the Bi-2223 crystal structure and solved completely as a consequence of the absent of the secondary phases. The diffraction line intensities belonging to the high-Tc phase systematically increase with the enhancement of the annealing temperature up to 800 °C beyond which they begin to decrease again due to the deterioration of the texturing and crystallinity. These evidences are strongly favored by the change of both the crystallite size and the cell constant parameters (a and c) against the annealing temperature.
- As for the microstructural examinations, the sample prepared at 800 °C for the annealing duration of 48 h

obtains the best, smoothest and least weak links between the superconducting grains (densest) surface morphology. After the critical annealing temperature point of 800 °C, the excess (more and more) Gd impurities start to penetrate into the crystal structure and thus surface morphology recrudesces seriously.

- The mechanical characteristics such as the Vickers microhardness, elastic modulus, yield strength and fracture toughness ascend with the diffusion annealing temperature up to 800 °C but reduce continuously with the applied indentation test loads. According to the results obtained, two important findings are extracted. (I) the microstructural properties improve with the annealing temperature and (II) each sample exhibits the standard *ISE* behaviour. This is in corresponding to the fact that the applied load is enough to produce both the elastic and plastic deformation in the superconducting system as a consequence the elastic recovery.
- All the experimental evidences indicate that the diffusion annealing temperature breaking point of the harmony between Gd diffused Bi-2223 layers is determined to be shortly after 800 centigrade degree.

Acknowledgments One of the authors, Gurcan Yildirim, dedicates this study to his father, Ismail Yildirim, on the occasion of his 59th Birthday.

References

1. M. Runde, IEEE Trans. Appl. Supercond. **5**, 813–816 (1995)
2. A. Godeke, D. Cheng, D.R. Dietderich, C.D. English, H. Felice, C.R. Hannaford, S.O. Prestemon, G. Sabbi, R.M. Scanlan, Y. Hikichi, J. Nishioka, T. Hasegawa, IEEE Trans. Appl. Supercond. **18**, 516–519 (2008)
3. S.E. Mousavi Ghahfarokhi, M. Zargar Shoushtari, Phys. B **405**, 4643–4649 (2010)
4. S. Bal, M. Dogruer, G. Yildirim, A. Varilci, C. Terzioglu, Y. Zalaoglu, J. Supercond. Nov. Magn. **25**, 847–856 (2012)
5. H. Zhang, H. Sato, Phys. Rev. Lett. **70**, 1697–1699 (1993)
6. G. Yildirim, A. Varilci, M. Akdogan, C. Terzioglu, J. Mater. Sci: Mater. El. **23**, 928–935 (2012)
7. C.K. Rhee, C.J. Kim, H.G. Lee, I.H. Kuk, J.M. Lee, I.S. Chang, C.S. Rim, P.S. Han, S.I. Pyun, D.Y. Won, Jpn. J. Appl. Phys. **28**, L1137–L1139 (1989)
8. K.A. Sarkar, I. Maartense, T.L. Peterson, B. Kumar, J. Appl. Phys. **66**, 3717–3722 (1989)
9. G. Yildirim, S. Bal, E. Yucel, M. Dogruer, M. Akdogan, A. Varilci, C. Terzioglu, J. Supercond. Nov. Magn. **25**, 381–390 (2012)
10. M. Dogruer, G. Yildirim, E. Yucel, C. Terzioglu, J. Mater. Sci: Mater. El. **23**, 1965–1970 (2012)
11. M. Dogruer, F. Karaboga, G. Yildirim, C. Terzioglu, O. Ozturk, J. Mater. Sci: Mater. El. (2013). doi:10.1007/s10854-013-1152-z
12. P.B. Allen, Y.E. Picket, H. Krakauer, Phy. Rev. B **37**, 7482–7490 (1988)
13. S. Martin, M. Gurvitch, C.E. Rice, A.F. Hebard, P.L. Gammel, R.M. Fleming, A.T. Fiory, Phys. Rev. B **39**, 9611–9613 (1989)
14. D.M. Newns, P.C. Pattnaik, C.C. Tsuei, Phys. Rev. B **43**, 3075–3084 (1991)
15. K. Levin, J.H. Kim, J.P. Lu, Q. Si, Physica C **175**, 449–522 (1991)
16. P.A. Lee, N. Read, Phys. Rev. Lett. **58**, 2691–2694 (1987)
17. O. Gorur, C. Terzioglu, A. Varilci, M. Altunbas, Supercond. Sci. Technol. **18**, 1233–1237 (2005)
18. M.B. Turkoz, S. Nezir, C. Terzioglu, A. Varilci, G. Yildirim, J. Mater. Sci: Mater. El. **24**, 896–905 (2013)
19. P.M. Sarun, S. Vinu, R. Shabna, A. Biju, U. Syamaprasad, Mater. Lett. **62**, 2725–2728 (2008)
20. G. Yildirim, E. Yucel, S. Bal, M. Dogruer, A. Varilci, M. Akdogan, C. Terzioglu, Y. Zalaoglu, J. Supercond. Nov. Magn. **25**, 231–237 (2012)
21. A. Biju, R.P. Aloysius, U. Syamaprasad, Supercond. Sci. Technol. **18**, 1454–1459 (2005)
22. V.G. Prabitha, A. Biju, R.G. Abhilashkumar, P.M. Sarun, R.P. Aloysius, U. Syamaprasad, Physica C **433**, 28–36 (2005)
23. N.T. Mua, A. Sundaresan, N.K. Man, D.D. Dung, Bull. Mater. Sci. 2013; In press
24. K. Kocabas, O. Ozkan, O. Bilgili, Y. Kadioglu, H. Yılmaz, J. Supercond. Nov. Magn. **23**, 1485–1492 (2010)
25. A. Ianculescu, M. Gartner, B. Despax, V. Bley, Th Lebey, R. Gavrila, M. Modreanu, Appl. Surf. Sci. **253**, 344–348 (2006)
26. M. Dogruer, O. Gorur, F. Karaboga, G. Yildirim, C. Terzioglu, Powder Technol. **246**, 553–560 (2013)
27. G. Yildirim, S. Bal, A. Varilci, J. Supercond. Nov. Magn. **25**, 1655–1663 (2012)
28. G. Yildirim, J. Alloy, Compd. **578**, 526–535 (2013)
29. M.R. Presland, J.L. Tallon, R.G. Buckley, R.S. Liu, N.E. Floer, Physica C **176**, 95–105 (1991)
30. K. Takita, T. Ohshima, Physica C **757**, 185–189 (1991)
31. S. Vinu, P.M. Sarun, A. Biju, R. Shabna, P. Guruswamy, U. Syamaprasad, Supercond. Sci. Technol. **21**, 045001–045005 (2008)
32. S. Vinu, P.M. Sarun, R. Shabna, A. Biju, U. Syamaprasad, Mater. Lett. **62**, 4421–4424 (2008)
33. R. Shabna, P.M. Sarun, S. Vinu, A. Biju, U. Syamaprasad, Supercond. Sci. Technol. **22**, 045016–045022 (2009)
34. P.M. Sarun, S. Vinu, R. Shabna, A. Biju, U. Syamaprasad, J. Alloy, Compd. **472**, 13–17 (2009)
35. A. Biju, P.M. Sarun, R.P. Aloysius, U. Syamaprasad, J. Alloy, Compd. **454**, 46–51 (2008)
36. A. Yildiz, K. Kocabas, G.B. Akyuz, J. Supercond. Nov. Magn. **25**, 1459–1467 (2012)
37. C. Terzioglu, A. Varilci, I. Belenli, J. Alloy, Compd. **478**, 836–841 (2009)
38. A. Matsumoto, H. Kumakura, H. Kitaguchi, H. Fujii, K. Togano **382**, 207–212 (2002)
39. Q. Li, D. Shi, X.B. Zhu, L. Wang, T. Yamashita, S. Cooper, IEEE T. Appl. Supercon. **21**, 160–163 (2011)
40. M. Dogruer, O. Gorur, Y. Zalaoglu, O. Ozturk, G. Yildirim, A. Varilci, C. Terzioglu, J. Mater. Sci: Mater. El. **24**, 352–361 (2013)
41. E.H. Brandt, Rep. Prog. Phys. **58**, 1465–1594 (1995)
42. D. Dew-Hughes, Phil. Mag. **30**, 293–305 (1974)